

# MULTIFUNCTIONAL STRUCTURES FOR SPACECRAFT ATTITUDE CONTROL

Vedant\*, Albert E. Patterson†, James T. Allison\*†

A new attitude control system called Multifunctional Structures for Attitude Control (MSAC) is explored in this paper. This system utilizes deployable structures to provide fine pointing and large slewing capabilities for spacecraft. These deployable structures utilize distributed actuation, such as piezoelectric strain actuators, to control flexible structure vibration and motion. A related type of intelligent structure has been introduced recently for precision spacecraft attitude control, called Strain Actuated Solar Arrays (SASA). MSAC extends the capabilities of the SASA concept such that arbitrarily large angle slewing can be achieved at relatively fast rates, thereby providing a means to replace Reaction Wheel Assemblies and Control Moment Gyroscopes. MSAC utilizes actuators bonded to deployable panels, such as solar arrays or other structural appendages, and bends the panels to use inertial coupling for small-amplitude, high-precision attitude control and active damping. In addition to presenting the concept, we introduce the operational principles for MSAC and develop a lumped low-fidelity Hardware-in-the-Loop (HIL) prototype and testbed to explore them. Some preliminary experimental results obtained using this prototype provided valuable insight into the design and performance of this new class of attitude control systems. Based on these results and developed principles, we have developed useful lumped-parameter models to use in further system refinement.

## INTRODUCTION

An Attitude Control System (ACS) is a critical spacecraft sub-system, required for proper functioning and positioning.<sup>1-3</sup> Several mission classes, such as space observatories,<sup>4,5</sup> synthetic-aperture radar (SAR),<sup>6,7</sup> and deep space missions<sup>8,9</sup> require a precise, accurate, and reliable ACS as essential technology. However, one of the problems with existing ACS systems is that they can produce a significant amount of vibration in the system which will need to be damped or dissipated or accounted for within the control system; this has been the topic of several studies.<sup>2,10-15</sup> Missions that require a more stable spacecraft platform (e.g., Hubble<sup>16,17</sup>) also utilize passive vibration isolation systems to have improved pointing accuracy. The collection of high-quality scientific data depends on fast and accurate reorientation and jitter reduction.<sup>18-21</sup> Therefore, high-precision attitude control is crucial for useful space data gathering.

Recent works have suggested that strain-actuated solar arrays (SASA) have the potential to achieve the positioning goals effectively by using distributed internal actuation across SAs (or other structural appendages).<sup>19</sup> One practical method for accomplishing this internal actuation is with

---

\*Department of Aerospace Engineering, University of Illinois at Urbana-Champaign, 104 S. Wright St., Urbana, IL 61801

†Department of Industrial and Enterprise Engineering, University of Illinois at Urbana-Champaign, 104 S. Mathews Ave., Urbana, IL 61801

Copyright (c) 2020 by Authors. This paper is released for publication to the American Astronautical Society in all forms.

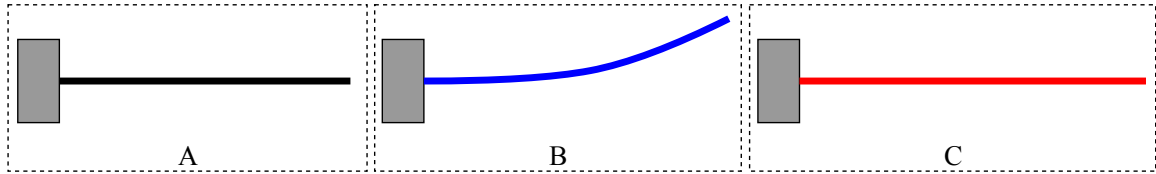


**Figure 1:** An illustration of one possible instantiation of the two types of strain that can produce secular attitude variation using the MSAC design: 1)  $A \rightarrow B$  and 2)  $A \rightarrow C$ .

piezoelectric actuators bonded to SAs.<sup>22</sup> While this control architecture performs well, a key drawback of the SASA technology is the reliance on other ACS to produce coarse, large-angle slewing. The most commonly used ACS for large-angle slewing are Reaction Wheel Assemblies (RWAs)<sup>23,24</sup> and Control Moment Gyroscopes (CMGs).<sup>2,25</sup> In a previous work,<sup>26</sup> we introduced a major expansion of the SASA concept which utilized the deployable structures to provide large-angle slewing in addition to jitter reduction. This extension of SASA principles was called Multifunctional Structures for Attitude Control (MSAC). These additional capabilities allow MSAC to replace conventional ACS technologies, thereby eliminating a key source of vibrational noise onboard spacecraft, while reducing the mass, volume and power budget of the ACS simultaneously. The compliant and distributed actuator based MSAC system will also have no sliding failure modes, and will be robust to individual actuator failure.

In this paper, we provide a brief introduction to the mechanisms and controls that enable arbitrary large slews, then discuss some previous simulation studies for the lumped model MSAC concept. We then describe a roller bearing based Hardware-in-the-Loop (HIL) testbed and conclude with a HIL test of a lumped model prototype for MSAC.

## MSAC SYSTEM OVERVIEW

The MSAC system utilizes existing deployable structures/appendages (such as solar arrays or radiators) as multifunctional devices, as demonstrated in Figure 1. This multi-role use of the solar panels extends their utility with a low mass penalty while increasing spacecraft ACS reliability. MSAC adds completely new functionality to SASA systems: Execution of arbitrarily-large spacecraft rotations (secular motion) with no sliding contacts in the ACS.

### Operating principles

To produce secular motion, we propose the utilization of transverse oscillations of the deployable panels combined with moment of inertia (MOI) reconfigurations. Both oscillations and reconfigurations are achieved by exercising the same set of distributed actuators. Strategic adjustments to MOI between transverse oscillations produce a secular change in attitude. One mechanism for changing MOI is to induce longitudinal strains, increasing or decreasing the MOI about the vehicle axis of rotation. To illustrate one possible instantiation of the MSAC concept, the two constituent phases are illustrated using a single axis of rotation MSAC system as follows:

1. Strain deployable structures for jitter control or for producing small slew maneuvers in the transverse panel direction. This is illustrated in Fig. 1, straining from the elastic equilibrium position (A) to the displaced position (B).
2. Strain deployable structures to alter inertial properties, seen in Fig. 1, straining from rest (A) to (C).

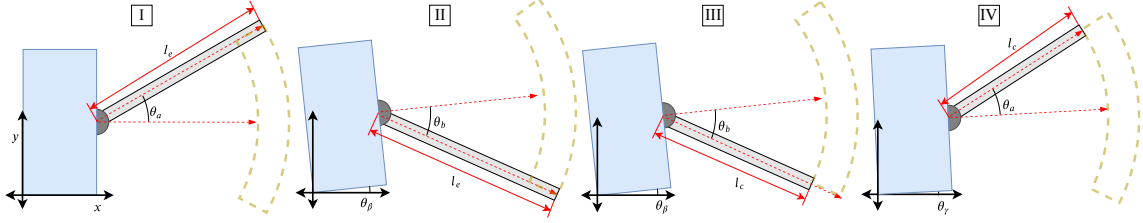


**Figure 2:** MSAC system demonstration with the non-holonomic trajectories. The reachable space for the appendage/deployable panel can be seen as the dashed yellow annulus ring sector.

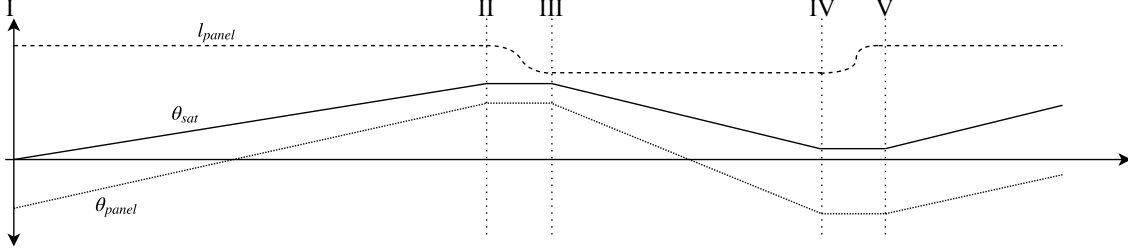


**Figure 3:** The trajectory plot of key state vectors during the different phases is shown in the plot, with the satellite attitude angle depicted as a solid line, the angle of the panel with respect to the body depicted as a dotted line, and length of the panel as a dashed line.

The latter element is a nonlinear behavior that allows the ACS to ‘reset’ between movements, producing a secular variation in attitude. From a dynamical system perspective, MSAC utilizes trajectories that are non-holonomic. Next, we briefly discuss the peak slew rates for a lumped MSAC prototype, a more detailed derivation of the non-holonomic trajectory is presented in Reference.<sup>27</sup>

### Performance of Lumped MSAC

$$I_{\text{sat}}(\theta_\gamma) = (I_e - I_c)(\theta_a - \theta_b), \quad (1)$$

$$\theta_\gamma = \frac{(I_e - I_c)}{I_{\text{sat}}}(\theta_a - \theta_b), \quad (2)$$

A simplified illustration of the MSAC cycle is shown in Fig. 2. It can be seen that at the end of this cycle (Phase IV), the satellite body has rotated by a small angle  $\theta_\gamma$ , while the panels have been reset back to the same relative orientation with respect to the spacecraft as in Phase I ( $\theta_a$ ). The average angular velocity of the attitude maneuver can be quantified using the following linear approximation:

$$\omega_\gamma \approx \frac{\theta_\gamma}{\Delta t} = \frac{(I_e - I_c)(\theta_a - \theta_b)}{I_{\text{sat}}\Delta t}, \quad (3)$$

where  $\Delta t = t_{bc} + t_{be} + t_e + t_c$  is the time required to perform one complete cycle (Phase I through Phase IV), as illustrated in Fig. 2.

### LUMPED MSAC PROTOTYPE

The system described here is a bulk, low-cost, low-fidelity version to be used to explore the theory and assumptions and develop more refined prototyping and testing methods around MSAC

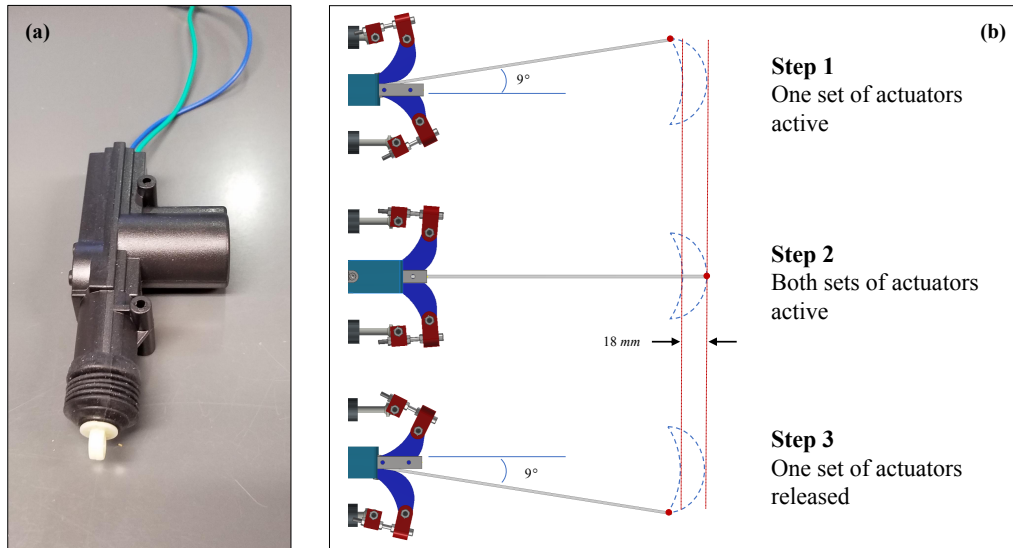


**Figure 4:** (a) automatic car door electric actuator ( $\delta = 20 \text{ mm}$  and  $F = 60 \text{ N}$ ) used to drive the prototype and (b) map of MSAC-like motion of the panels for the prototype design (total sweep  $18^\circ$  and  $18 \text{ mm}$  (6%) extension)

as discussed above. It is a hardware-in-the-loop (HIL) device, which gives more realistic and useful data than a simulation, including reproducing the physical maneuvers expected from MSAC.

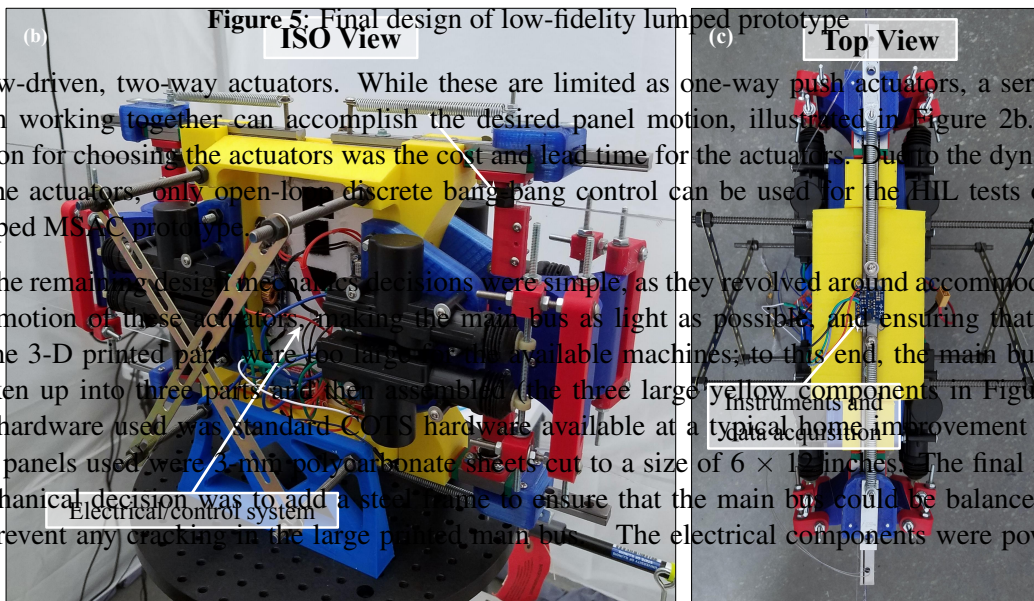
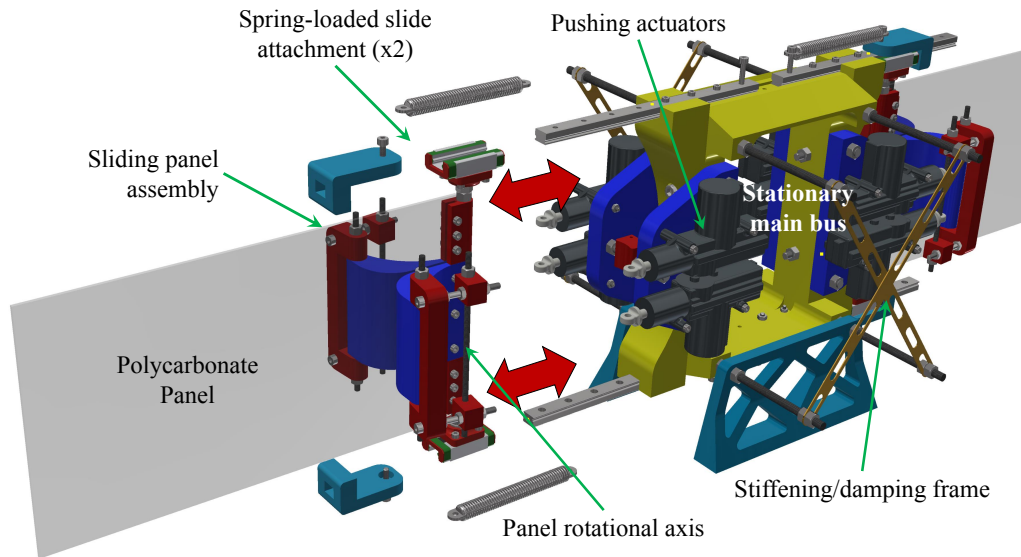
The prototype and testbed discussed in this report are at the low-fidelity, HIL phase (i.e., the first serious testing phase after concept exploration). Many design decisions for the system will be made or refined based on data collected at this phase.

### High-Level Requirements

In addition to MSAC-like motion,<sup>27</sup> several requirements were established for the construction of a prototype and a feasible testbed, including: 1) The prototype must be as low-cost as possible, using standard hardware and 3-D printed parts for as much of the construction as possible; 2) The panels must move in a controllable way; 3) There must be no wires or cables to the ground (i.e., the prototype must effectively float and have self-contained power and controllers); 4) The testbed must be simple and low-cost while being model-friendly; 5) Testing must be done in a clean environment. These were all satisfied during the design and building of the prototype and testbed, as shown in the following sections. Requirement 1 imposed several other sub-requirements, including that no individual part could be larger than the print area of the largest printer available (i.e.,  $200 \text{ mm} \times 220 \text{ mm} \times 180 \text{ mm}$ ), that the hardware all had to be commercial off-the-shelf (COTS), and that printing direction and part density must be considered in design as it can affect the structural integrity of the prototype.

### Prototype Design Approach, Assumptions, and Simplifications

Due to the freedom and low cost provided by using mainly 3-D printed plastic components, the most vital design decision was the method for moving the panels during operation. It was decided that linear electric actuators would be used, as they are reliable, powerful, and low cost. After investigating the cost and type needed, it became clear that automatic car door locking actuators (Figure 2a) was the best option, as they are fast-acting, strong, and less than 5% of the cost of



screw-driven, two-way actuators. While these are limited as one-way push actuators, a series of them working together can accomplish the desired panel motion, illustrated in Figure 2b. The reason for choosing the actuators was the cost and lead time for the actuators. Due to the dynamics of the actuators, only open-loop discrete bang-bang control can be used for the HIL tests of the lumped MSAC prototype.

The remaining design mechanics decisions were simple, as they revolved around accommodating the motion of these actuators, making the main bus as light as possible, and ensuring that none of the 3-D printed parts were too large for available machines; to this end, the main bus was broken up into three parts and then assembled (the three large yellow components in Figure 5). All hardware used was standard COTS hardware available at a typical home improvement store. The panels used were 3-mm polycarbonate sheets cut to a size of  $6 \times 18$  inches. The final major mechanical decision was to add a steel frame to ensure that the main bus could be balanced and to prevent any cracking in the large printed main bus. The electrical components were powered

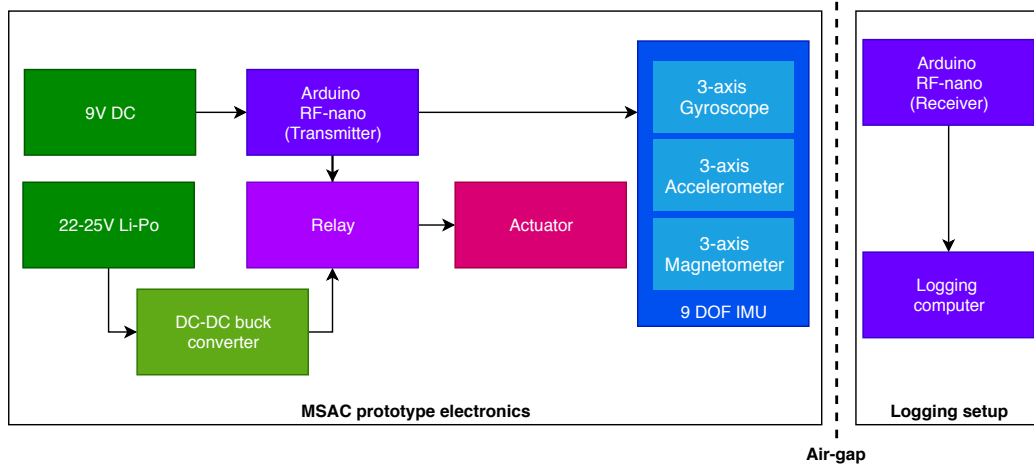
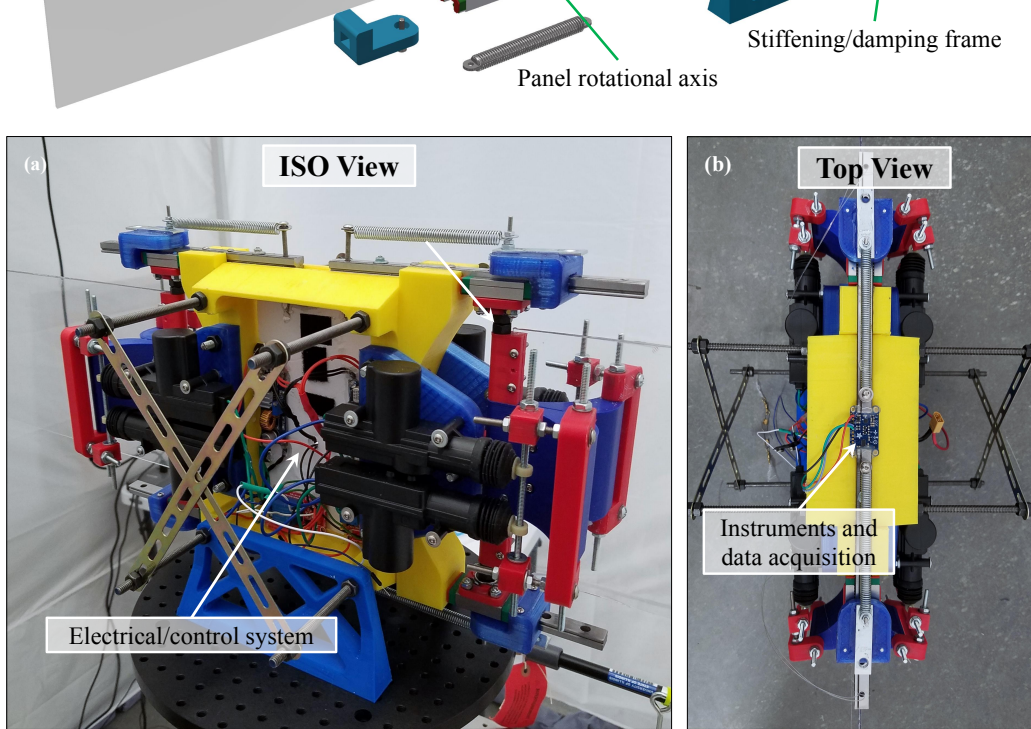


Figure 6: Electrical setup for the MSAC prototype.



**Figure 7:** MSAC prototype from (a) isometric and (b) top views to show the mechanical details and location of instruments

using a 22–25 V lithium polymer battery. The linear actuators were supplied with 12 V 5 A power using a buck converter. All sensors and control signals operated at 5 V, provided by a 9 V COTS battery; this supply was independent of the main 22 V battery to prevent any electrical interference between the high-power and sensitive low-power instruments. An Arduino RF-nano produced all control signals and provided sensor logging. The control signals were used to switch high-speed relays to control the supply to the linear motors. The sensor data was transmitted wirelessly using an RF transceiver. The data was received using another Arduino RF-nano connected to a personal computer and was logged. A summary of the electrical setup can be seen in Fig. 6

The final design is presented in Figure 5a, including the moving panels, main bus, etc., with the constructed prototype shown in Figures 7b-c.

Additionally, the prototype also has a COTS nine-axis Inertial Measurement Unit (IMU) consisting of a three-axis accelerometer, magnetometer, and gyroscope to measure the attitude slews during tests. The system is powered using Lithium polymer batteries, and the sensor data is wirelessly transmitted to an external data logger. This allows for minimal external torques on the system under test and can be used in subsequent higher-fidelity tests using air bearings to minimize the contribution of friction.

## HIL TESTBED

As previously discussed, the testbed was required to present a clean environment and allow the prototype to complete its mission at a low cost. To establish a clean environment, a vinyl tent was set up in a high bay area as a quasi-cleanroom (Figure 8a). The tent was lightly pressurized using an in-line fan and charcoal air filter with a diffuser to prevent air currents inside of the tent (Figure 8b). The tent was sealed at the bottom using sandbags after setup and observed to bow out lightly from the pressure difference after about one minute of the air system running.

To construct the test-bed itself, two flat, stable, clean surfaces were obtained: 1) an optical table,

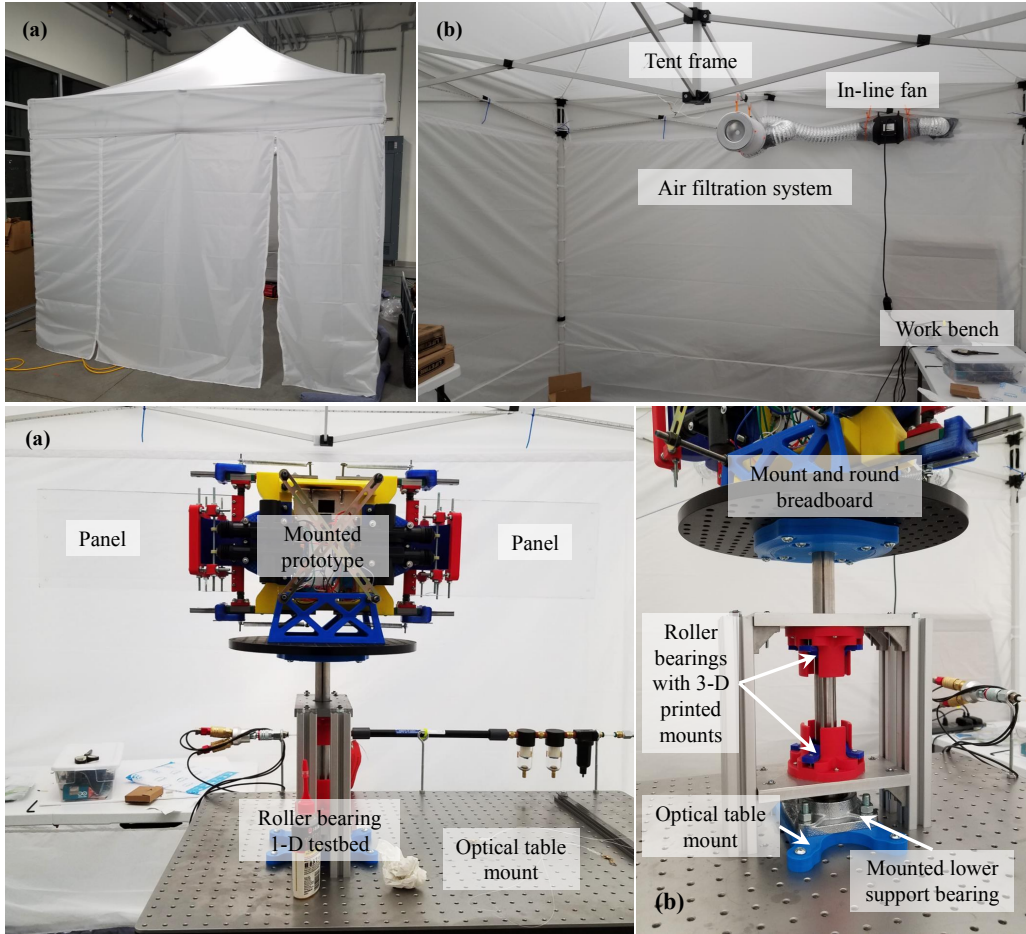


**Figure 9:** 1-D roller bearing testbed (a) overall design and (b) detailed close-up view

and 2) a circular optical breadboard (Figure 9a). To connect the two, a 1-D roller bearing support was designed and built, using a mounted bearing on the bottom and shaft supported by two roller bearings. The frame was built from aluminum plates and extruded aluminum framing, as shown in Figure 9b, supported by 3-D printed supports for the bearings themselves (Figure 9b). The bearings were well-lubricated in preparation for any tests.

## RESULTS

Here we present and discuss the data logged from the IMU sensor for the slewing test performed on the HIL testbed described in the previous section. Attitude slews on the one axis roller bearing test-bed were performed in both clockwise and counterclockwise directions. Performing slews in both directions demonstrates that prototype rotation could not be due only rotation table misalignment.

Due to constraints imposed by the design of the current system, such as the compliance of the deployable panels and discreet control of the linear actuators, all HIL tests were performed using open-loop bang-bang control trajectories. Such control trajectories produce significantly larger vibrational noise on the satellite during slews, but demonstrate the expected overall motion. Given

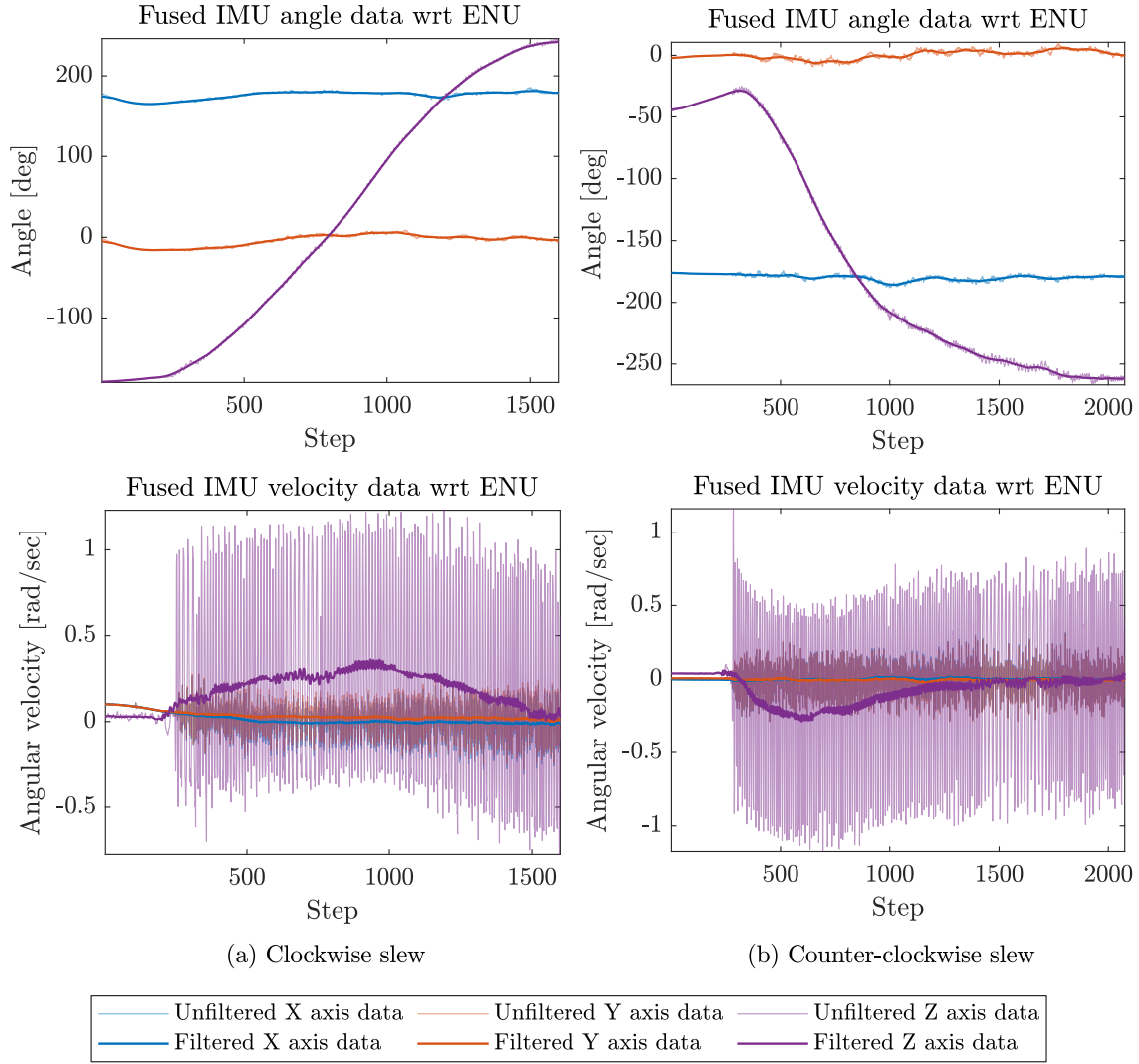


**Figure 10:** Hardware in the loop Euler angle and angular rate data during HIL slews about the local z-axis, where the gravity vector is along negative z-axis (“East-North-Up” ENU frame).

the nature of the current open-loop control trajectories being used for the tests, the frequency of actuation for the linear actuators was constrained to be faster than the time period of the first natural frequency of the deployable panels, which then sets the peak slew rate of the prototype.

### **Clockwise slew**

Figure 10a shows the angular velocity data from the fused IMU estimates for the clockwise slew. The darker line is a low pass filtered measurement of the data-logged by the system, while the dashed line is the unfiltered measurement. The angle and velocity estimates were obtained using the gyroscope and accelerometer sensors; the magnetometer data was not reliable due to the large magnetic noise produced using the linear actuators. The attitude solution was obtained from the “imufilter” function provided by the robotics and sensing toolbox in MATLAB. The filters provide orientation and angular rate estimates in the “East-North-Up” local frame of reference. The orientation is reported as quaternions which are then converted to Euler angles using the “XYZ” notion.

Due to the low fidelity and open-loop nature of the control signal provided to the drive actuators, the vibrations experienced on the central satellite body is significantly higher than what would be expected in a distributed system. Despite larger vibrations, a clear attitude slew can be seen in the gyroscope data.

### **Counter-clockwise slew**

Figure 10b shows the angular velocity data from the fused IMU estimates for the counter-clockwise slew. A similar trend-line is seen for both slews, which indicated that the slews are not due to misalignment and frictional force interactions.

## **FUTURE WORK**

The current work demonstrates a lumped actuation hardware representation of the MSAC concept; future work will realize the same motions using distributed actuators embedded in deployable elastic panels which can produce similar motions. The magnitude of the peak slew rate is a function of the peak deflections ( $\delta$ ) produced and the frequency of actuation ( $f$ ). The peak slew rate ( $\omega_{\max}$ ) can be approximated using Eq. (4).

$$\omega_{\max} = \delta \cdot f \quad (4)$$

A more detailed discussion of the equation above can be found in Reference.<sup>27</sup>

Although in the distributed compliant realization of MSAC the peak deflections  $\delta$  will be smaller than the lumped model realization, the frequency of operation  $f$  will be significantly higher, thereby having similar peak slew rates. Figure 11 shows a physical realization of the actuators capable of compliant, low deflection high frequency MSAC prototype.<sup>27</sup> This actuator depends on piezoelectric elements (yellow element in Fig. 11), which has significantly faster response times and lower magnetic noise.

---

The HIL test video is available at <http://hdl.handle.net/2142/106081>

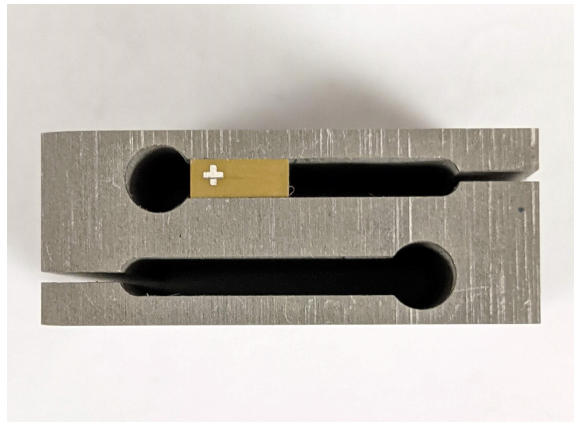


**Figure 11:** Compliant actuator for high fidelity MSAC prototype, using piezoelectric elements (yellow) for actuation. Total height of the actuator depicted is 10mm.

### Applications

The future development of this technology will include an expansion of its multi-functional capabilities. Currently, MSAC can make dual use of any deployable panels, thereby reducing the volume and mass budget of an ACS. Combining the MSAC with deployable panels developed for the ISARA<sup>28</sup> mission allows for further mass and volume savings for the bus functionality while providing secondary benefits, such as better alignment of panels for high-frequency communication or Synthetic Aperture Radar (SAR) missions.

### CONCLUSION

The feasibility of the MSAC concept has been shown through both multi-body simulations and low-level HIL testing. The large slews enabled by MSAC enable MSAC to work in conjunction with or replace conventional ACS, thus making it an alternative to RWAs and CMGs. A more detailed discussion of the impact of MSAC on various mission classes has also shown that there can be potential mass and volume savings.<sup>29</sup>

MSAC is the subject of US provisional patent filing 62/862,412 and has been filed internationally through the Patent Cooperation Treaty.

### ACKNOWLEDGMENTS

This material is based upon work supported by the National Science Foundation under Grant No. CMMI-1653118.

### REFERENCES

- [1] S. Yin, B. Xiao, S. X. Ding, and D. Zhou, "A Review on Recent Development of Spacecraft Attitude Fault Tolerant Control System," *IEEE Transactions on Industrial Electronics*, Vol. 63, May 2016, pp. 3311–3320, 10.1109/tie.2016.2530789.
- [2] V. Lappas, W. Steyn, and C. Underwood, "Attitude control for small satellites using control moment gyros," *Acta Astronautica*, Vol. 51, July 2002, pp. 101–111, 10.1016/s0094-5765(02)00089-9.
- [3] J. Li, M. Post, T. Wright, and R. Lee, "Design of Attitude Control Systems for CubeSat-Class Nanosatellite," *Journal of Control Science and Engineering*, Vol. 2013, 2013, pp. 1–15, 10.1155/2013/657182.
- [4] G. A. Beals, R. C. Crum, H. J. Dougherty, D. K. Hegel, J. L. Kelley, and J. J. Rodden, "Hubble Space Telescope precision pointing control system," *Journal of Guidance, Control, and Dynamics*, Vol. 11, Mar. 1988, pp. 119–123, 10.2514/3.20280.

- [5] A. J. Bronowicki, "Vibration Isolator for Large Space Telescopes," Journal of Spacecraft and Rockets, Vol. 43, Jan. 2006, pp. 45–53, 10.2514/1.12036.
- [6] P. Rosen, S. Hensley, I. Joughin, F. Li, S. Madsen, E. Rodriguez, and R. Goldstein, "Synthetic aperture radar interferometry," Proceedings of the IEEE, Vol. 88, Mar. 2000, pp. 333–382, 10.1109/5.838084.
- [7] R. M. Duren, E. Wong, B. Breckenridge, S. J. Shaffer, C. Duncan, E. F. Tubbs, and P. M. Salomon, "Metrology, attitude, and orbit determination for spaceborne interferometric synthetic aperture radar," Acquisition, Tracking, and Pointing XII (M. K. Masten and L. A. Stockum, eds.), SPIE, July 1998, 10.1117/12.317529.
- [8] K. Lau, S. Lichten, L. Young, and B. Haines, "An innovative deep space application of GPS technology for formation flying spacecraft," Guidance, Navigation, and Control Conference, American Institute of Aeronautics and Astronautics, July 1996, 10.2514/6.1996-3819.
- [9] W. H. Blume, "Deep Impact Mission Design," Space Science Reviews, Vol. 117, Mar. 2005, pp. 23–42, 10.1007/s11214-005-3386-4.
- [10] Q. Hu and G. Ma, "Variable structure control and active vibration suppression of flexible spacecraft during attitude maneuver," Aerospace Science and Technology, Vol. 9, June 2005, pp. 307–317, 10.1016/j.ast.2005.02.001.
- [11] G. Song and B. N. Agrawal, "Vibration suppression of flexible spacecraft during attitude control," Acta Astronautica, Vol. 49, July 2001, pp. 73–83, 10.1016/s0094-5765(00)00163-6.
- [12] Q. I. Hu, Z. Wang, and H. Gao, "Sliding mode and shaped input vibration control of flexible systems," IEEE Transactions on Aerospace and Electronic Systems, Vol. 44, Apr. 2008, pp. 503–519, 10.1109/taes.2008.4560203.
- [13] A. Molter, O. A. A. da Silveira, V. Bottega, and J. S. O. Fonseca, "Integrated topology optimization and optimal control for vibration suppression in structural design," Structural and Multidisciplinary Optimization, Vol. 47, No. 3, 2013, pp. 389–397, 10.1007/s00158-012-0829-x.
- [14] H.-S. Yoon, "Optimal shape control of adaptive structures for performance maximization," Structural and Multidisciplinary Optimization, Vol. 48, No. 3, 2013, pp. 571–580, 10.1007/s00158-013-0917-6.
- [15] G. van der Veen, M. Langelaar, and F. van Keulen, "Integrated topology and controller optimization of motion systems in the frequency domain," Structural and Multidisciplinary Optimization, Vol. 51, No. 3, 2015, pp. 673–685, 10.1007/s00158-014-1161-4.
- [16] C. L. Foster, M. L. Tinker, G. S. Nurre, and W. A. Till, "Solar-array-induced disturbance of the Hubble Space Telescope pointing system," Journal of Spacecraft and Rockets, Vol. 32, July 1995, pp. 634–644, 10.2514/3.26664.
- [17] P. Y. Bely, O. L. Lupie, and J. L. Hershey, "Line-of-sight jitter of the Hubble Space Telescope," Space Astronomical Telescopes and Instruments II (P. Y. Bely and J. B. Breckinridge, eds.), SPIE, Nov. 1993, 10.1117/12.158800.
- [18] A. H. de Ruiter, C. Damaren, and J. R. Forbes, Spacecraft dynamics and control: an introduction. Chichester, West Sussex: John Wiley & Sons, 1 ed., Jan. 2013.
- [19] C. M. Chilan, D. R. Herber, Y. K. Nakka, S. J. Chung, F. T. Allison, J. B. Aldrich, and O. S. Alvarez-Salazar, "Co-Design of strain-actuated solar arrays for spacecraft precision pointing and jitter reduction," AIAA Journal, Vol. 55, Sept. 2017, pp. 3180–3195, 10.2514/1.J055748.
- [20] S. J. C. Dyne, D. E. L. Tunbridge, and P. P. Collins, "The vibration environment on a satellite in orbit," High Accuracy Platform Control in Space, IEE Colloquium on, IET, 1993, pp. 12–1.
- [21] S. Arnon and N. S. Kopeika, "Laser satellite communication network-vibration effect and possible solutions," Proceedings of the IEEE, Vol. 85, No. 10, 1997, pp. 1646–1661, 10.1109/5.640772.
- [22] E. Crawley and J. de Luis, "Use of piezoelectric actuators as elements of intelligent structures," AIAA journal, Vol. 25, No. 10, 1987, pp. 1373–1385, 10.2514/3.9792.
- [23] W.-Y. Zhou and D.-X. Li, "Design and analysis of an intelligent vibration isolation platform for reaction/momentum wheel assemblies," Journal of Sound and Vibration, Vol. 331, June 2012, pp. 2984–3005, 10.1016/j.jsv.2012.02.018.
- [24] Z. Zhang, G. S. Aglietti, and W. Ren, "Coupled microvibration analysis of a reaction wheel assembly including gyroscopic effects in its acceleration," Journal of Sound and Vibration, Vol. 332, Oct. 2013, pp. 5748–5765, 10.1016/j.jsv.2013.06.011.
- [25] H. Yoon and P. Tsotras, "Spacecraft Adaptive Attitude and Power Tracking with Variable Speed Control Moment Gyroscopes," Journal of Guidance, Control, and Dynamics, Vol. 25, Nov. 2002, pp. 1081–1090, 10.2514/2.4987.
- [26] Vedant, A. Ghosh, O. S. Alvarez-Salazar, and J. T. Allison, "Impact of Strain-Actuated Attitude Control Systems for Variant Mission Classes," 70th International Astronautical Congress, No. C1.5.2, Washington D.C., United States, Oct. 2019.

- [27] Vedant and J. T. Allison, "Multifunctional Structures for Attitude Control," Vol. ASME 2019 Conference on Smart Materials, Adaptive Structures and Intelligent Systems of Smart Materials, Adaptive Structures and Intelligent Systems, 09 2019. V001T03A005, 10.1115/SMASIS2019-5565.
- [28] R. E. Hodges, M. J. Radway, A. Toorian, D. J. Hoppe, B. Shah, and A. E. Kalman, "ISARA-integrated solar array and reflectarray CubeSat deployable Ka-band antenna," 2015 IEEE International Symposium on Antennas and Propagation & USNC/URSI National Radio Science Meeting, IEEE, 2015, pp. 2141–2142.
- [29] Vedant, A. Ghosh, O. Alvarez-Salazar, and J. Allison, "Impact of Strain-Actuated Attitude Control Systems for Variant Mission Classes," 70th International Astronautical Congress 2019, IAC 2019, Proceedings of the International Astronautical Congress, IAC, International Astronautical Federation, IAF, 1 2019.